Eigenvectors of internal vibrations of C_{60}: Theory and experiment

R. Heid* and L. Pintschovius
Forschungszentrum Karlsruhe, Institut für Nukleare Festkörperphysik, P.O. Box 3640, D-76021 Karlsruhe, Germany

J. M. Godard
Laboratoire de Physique des Solides, Université de Paris-Sud, F-91405 Orsay Cedex, France
(Received 12 March 1997)

We have studied the eigenvectors of all internal modes of C_{60} up to 75 meV by inelastic neutron scattering. The experimental data are compared in detail with a state-of-the-art *ab initio* theory and a phenomenological model of the vibrational spectrum of C_{60}, respectively. We demonstrate that the momentum dependence of mode intensities obtained from measurements on single crystals as well as on powder samples represents a sensitive fingerprint of the eigenvectors which allows (i) unambiguous assignments of silent modes and (ii) discrimination of eigenvectors of modes belonging to the same symmetry class. The latter property can be used for stringent tests of theoretical models. Eigenvectors predicted by the *ab initio* theory are found to be in very satisfactory agreement with the experimental data, while those obtained from the phenomenological model turn out to be less reliable. We have also performed measurements to study the dispersion of the $H_g(1)$ mode in the low-temperature phase. We found that the data can be largely, although not fully, understood on the basis of a simple van der Waals ansatz for the intermolecular interactions. [S0163-1829(97)05934-1]

I. INTRODUCTION

The discovery of the fullerenes[1] and of a method[2] for the production of large quantities of fullerene solids has stimulated a great deal of experimental and theoretical studies. Within the fullerene family C_{60} keeps a prominent position primarily for the high symmetry of the C_{60} molecule which greatly facilitates theoretical computations and the interpretation of experimental data, but also because it is the only fullerene which can be grown in the form of large and nearly perfect single crystals. So C_{60} appears as an ideal testing ground for our understanding of the intramolecular binding forces and of their modification when C_{60} molecules form a solid. Indeed, numerous investigations have been devoted to the vibrational spectrum of the isolated C_{60} molecule or of the corresponding molecular solid. On the theoretical side, the studies are based on either *ab initio*[3–10] or semiempirical methods[11,12] or phenomenological models.[13–15] On the experimental side, several techniques have been used to characterize the vibrational properties, including Raman spectroscopy,[16–21] infrared spectroscopy,[16,22–24] high-resolution electron-energy-loss spectroscopy,[25] and inelastic neutron scattering.[26–30] In general, the agreement between calculated and observed frequencies was found to be very satisfactory or even excellent.

The good agreement between theory and experiment is true, of course, only if the assignment of the experimentally observed modes is correct and if the calculated displacement pattern is borne out by experiment. For the assignment problem optical spectroscopy was of great help as selection rules allow one to assign a certain frequency to a certain symmetry class of the eigenmodes. There are, however, more silent modes (32) than infrared- (4) or Raman- (10) active modes, so that optical spectroscopy can only partly solve the problem. In principle, inelastic neutron scattering allows one to unambiguously assign all the modes, but has so far not been used to this end, presumably for the following reasons: firstly, the determination of eigenvectors is traditionally based on single-crystal samples, but the available C_{60} crystals were too small for inelastic neutron-scattering experiments, and secondly, assignment of the modes requires their separation in energy which is difficult if not impossible to achieve for many of the C_{60} modes with present-day neutron spectrometers. In this paper, we demonstrate that inelastic neutron scattering is indeed a powerful tool for the eigenmode assignment at least for the lower part of the vibrational spectrum, where the necessary energy resolution can be achieved today. Our study benefited very much from recent progress in crystal growth, but as we will show more could have been done already with powder samples and using spectrometers with moderate resolution, provided measurements are made for many different momentum transfers.

A correct assignment means a correct labeling of experimental frequencies as the ith frequency of a certain symmetry class, e.g., T_{1u}. Without solving the assignment problem no meaningful comparison can be made between observed and calculated frequencies as it is well known that theories may be built which reproduce perfectly all experimental frequencies albeit many assignments are wrong. However, even if all assignments are made correctly there remains a problem: the displacement pattern of a mode belonging to a symmetry class with more than one member (which is the case for all but one of the C_{60} modes) is not determined by symmetry alone. Therefore, a good agreement between calculated and observed frequencies can be seen as satisfactory only in the case where the calculated displacement pattern is confirmed by experiment, too. Further we note that properties like the electron-phonon coupling strength directly depend on the mode eigenvectors, so that eigenvectors are an important input for theories aiming at a description of these quantities.[31]

Unfortunately, it is practically impossible to directly infer

the eigenvectors from the experimental data. Therefore, in the present paper, we adopt the strategy to check theoretically predicted eigenvectors by investigating the momentum dependence of the intensity in great detail. As will be shown, this momentum dependence is a very prominent fingerprint of a mode: it does not only allow one to unambiguously identify its symmetry class, but it provides also a sensitive test how well the eigenvectors are quantitatively predicted by theory. This is already true for data taken on powder samples, although to a lesser extent than for single crystal data.

For our comparison between theory and experiment we have chosen on the one hand an *ab initio* theory,[10] and on the other hand a phenomenological one.[13] We think that both theories are state of the art and are therefore representative of other theories of the same kind. We find that the two theories investigated differ not only in their agreement between calculated and observed frequencies, but also in their agreement between calculated and observed intensities. In other words, eigenvectors are predicted with uneven reliability.

When C_{60} molecules form a solid the intermolecular interaction modifies the spectrum of the internal vibrations: degeneracies are lifted and the modes show dispersion. Inelastic neutron scattering is, in principle, able to shed light also on these modifications. In practice, however, any attempt to unravel dispersion curves seems hopeless for all but the lowest internal mode [$H_g(1)$]. It turned out that even an investigation of the dispersion of the $H_g(1)$-related modes is extremely difficult and we could extract only summary information on this issue from this study.

Our paper is organized as follows: In Sec. II we derive the formulas needed to calculate the quantities observed in experiment. In Sec. III we give a brief survey of the experimental methods used in our study. In Sec. IV we make a detailed comparison between experimental and theoretical results, and Sec. V is devoted to the conclusions.

II. THEORY

A. Calculations of intramolecular modes

Because of its high icosahedral symmetry, the 174 internal vibrations of an isolated C_{60} molecule are grouped into 46 distinct modes. They consist of ten Raman-active (two A_g and eight H_g), four infrared-active (T_{1u}), and 32 silent modes, with excitation energies ranging from 33 to 195 meV (270 to 1580 cm^{-1}). Due to the strong covalent bonds between carbon atoms on the molecule, vibrations with predominant tangential displacements of the atoms are expected to possess higher energies, while the low-energy part of the spectrum will consist mainly of radial modes. In Fig. 1 we show displacement patterns of modes which are of relevance for our analysis.

In recent years, a large variety of theoretical methods have been applied to the calculation of the internal modes of C_{60}. They can be classified as *ab initio* methods, semiempirical methods, and phenomenological approaches. For the purpose of comparison with our experimental data, we have chosen two theories from both ends of this spectrum, namely an *ab initio* theory, which is parameter free, and a phenomenological model, which uses parameters determined by a fit to experimental data.

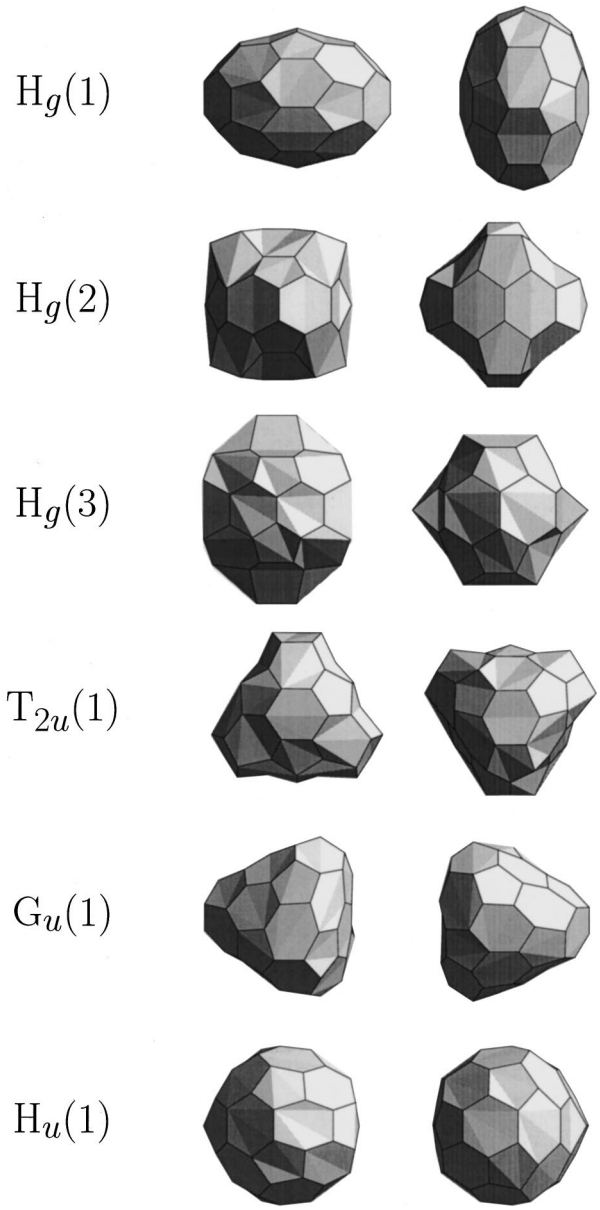

FIG. 1. Displacement patterns for five different eigenmodes of the C_{60} molecule. The elongations are strongly exaggerated for the sake of clarity. The left-hand and the right-hand figures correspond to extremal distortions following each other at time intervals $1/2\nu$. Eigenvectors are taken from the *ab initio* calculation of Bohnen *et al.* (Ref. 10).

The various first-principles methods applied to our problem are all based on the local-density approximation, but differ from each other by the computational scheme to extract phonon frequencies. Among these methods, *ab initio* molecular-dynamics simulations[3,4] are usually of relatively low accuracy. Calculations of the internal modes of an isolated C_{60} cluster have been carried out by Wang *et al.*[5] and Quong *et al.*[6] within all-electron schemes, and by Faulhaber *et al.*[7] and Jones *et al.*[8] using pseudopotential approaches, respectively. For the C_{60} solid, a density-functional perturbation approach has been applied by Giannozzi and Baroni,[9] whereas Bohnen *et al.*[10] used a frozen-phonon method. Frequencies predicted from these theories are summarized in Table I, and compared with the results of our experimental

TABLE I. Frequencies (in cm^{-1}) for internal modes of C_{60} up to 600 cm^{-1} (75 meV). Values obtained in the present experimental work agree very well with those published by Copley *et al.* (Ref. 30) and, after suitable modifications of assignments, with those from Coulombeau *et al.* (Ref. 28). They are compared with *ab initio* theories of Bohnen *et al.* (Ref. 10), Wang *et al.* (Ref. 5), Quong *et al.* (Ref. 6), Giannozzi and Baroni (Ref. 9), Jones *et al.* (Ref. 8), and Faulhaber *et al.* (Ref. 7), and with phenomenological models of Jishi *et al.* (Ref. 13), Feldman *et al.* (Ref. 14), and Onida and Benedek (Ref. 15). Raman- and infrared-active modes are denoted by R and IR, respectively. The last line shows the root-mean-square relative deviations of each model with respect to all 14 optically active modes (experimental data from Refs. 18 and 22).

Mode	Experiment			*Ab initio*						Phenomenology		
	This work	Ref. 28	Ref. 30	Ref. 10	Ref. 5	Ref. 6	Ref. 9	Ref. 8	Ref. 7	Ref. 13	Ref. 14	Ref. 15
$H_g(1)$ (R)	265	264	266	263	263	258	259	288	249	269	268	265
$T_{2u}(1)$	343	344	344	343	344	342	337	363		367	377	355
$G_u(1)$	350	355	352	348	356	356	349	374		385	346	330
$H_u(1)$	399	404	402	388	396	404	399	303		361	387	417
$H_g(2)$ (R)	431	432	429	422	432	439	425	437	421	439	438	408
$G_g(1)$	482	488	485	480	484	486	480	454		498	449	430
$A_g(1)$ (R)	493	488	490	481	483	478	495	582	459	492	483	496
$T_{1u}(1)$ (IR)	528	526	526	514	533	547	527	614	506	505	547	527
$H_u(2)$	535	536	534	527	534	539	530	510		543	521	488
$T_{2g}(1)$	553	563	553	543	550	547	548	514		541	573	640
$T_{1g}(1)$	563	563	565	563	566	580	564	661		501	584	568
$T_{1u}(2)$ (IR)	576	576	578	569	548	570	586	647	550	589	578	586
$G_g(2)$	570	576	569	570	564	571	566	517		626	612	660
rms (%)				2.1	2.6	2.0	2.0	8.6	4.6	1.8	3.8	3.0

investigation as discussed in Sec. IV. Only values for the 13 modes with energies less than 75 meV are shown in Table I, as this was the energy range accessible in our experiment. Generally, all-electron cluster and bulk approaches predict very similar frequencies, which agree well with experimental data, whereas results from cluster calculations based on the pseudopotential approximation exhibit larger deviations. This tendency is also found in the root-mean-square (rms) deviation of all calculated optical frequencies from values obtained in Raman[18] and IR (Ref. 22) studies (see Table I), which provides a measure for the average accuracy over the whole energy range of the vibrational spectrum.

Table I also contains results from three phenomenological calculations of the vibrational spectrum of a C_{60} cluster. Jishi *et al.*[13] employed a parametrization of the intramolecular interaction by a short-range force field with four longitudinal bond-stretching and four bond-angle-bending force constants. A seven parameter valence-force-field model including three- and four-body terms has been used by Feldman *et al.*,[14] while Onida and Benedek[15] applied a bond-charge model with only four adjustable parameters. All three calculations have incorporated experimental information about optical frequencies in their fit procedure to determine the adjustable parameters. This has considerably improved the accuracy of the predicted frequencies as compared to earlier approaches, which had to rely on parameters transfered from other materials[11] or extracted from quantum-chemical calculations.[12] As can been seen from Table I, the fit procedure usually results in a satisfactory description of the optical frequencies, but significant differences for the silent modes remain.

For our data analysis, we have used the results of Bohnen *et al.*[10] and the force-constant model of Jishi *et al.*[13] as representatives of the *ab initio* and of the phenomenological approach, respectively. Both theories have a similar accuracy with respect to the optical modes, but exhibit noticeable discrepancies for the silent modes, which partly affect the predicted order of the modes as a function of frequency.

B. Neutron-scattering cross section in the independent molecule approximation

In the solid, the interaction between C_{60} molecules is small compared to the on-ball interaction, and evokes only small dispersions of internal modes. As a consequence, the sum of the neutron-scattering intensities of phonons belonging to the same mode of the isolated molecule should be well described within the independent molecule approximation, where the intermolecular interaction is totally neglected.

Here we briefly summarize the relevant expressions for the scattering intensity of a dispersionless mode of a molecular crystal. The appropriate starting point for a coherent scatterer like carbon is the one-phonon coherent partial differential cross section, which in the case of energy-loss scattering has the form[32]

$$\frac{d^2\sigma}{d\Omega dE}=\frac{k_f}{k_i}\frac{\pi^2\sigma_c}{v_0 M}\frac{1+n(\omega)}{\omega}\sum_{\mathbf{G}}\sum_{\mathbf{q}\lambda}\delta(\mathbf{Q}-\mathbf{q}-\mathbf{G})\times\delta(\omega-\omega_{\mathbf{q}\lambda})|F_{\mathbf{q}\lambda}(\mathbf{Q})|^2. \quad (1)$$

Here, k_i, k_f are initial and final momenta of the neutron, $\mathbf{Q}=\mathbf{k}_i-\mathbf{k}_f$ is the momentum transfer to the sample, v_0 is the volume of the unit cell, σ_c is the coherent scattering cross section per atom, M is the mass of an atom, and $n(\omega)$ is the Bose factor. The summations are performed over all reciprocal-lattice vectors $\mathbf{G}$ and all normal modes $(\mathbf{q}\lambda)$, with wave vector $\mathbf{q}$ and frequency $\omega_{\mathbf{q}\lambda}$. The scattering intensity of a normal mode is determined by the structure factor

$$F_{\mathbf{q}\lambda}(\mathbf{Q})=\sum_{\mu} e^{-W_{\mu}(\mathbf{Q})}e^{-i\mathbf{Q}\mathbf{R}_{\mu}}\mathbf{Q}\mathbf{v}_{\mu}(\mathbf{q}\lambda), \tag{2}$$

where μ labels atoms within a unit cell, $\mathbf{R}_{\mu}$ is the equilibrium position vector, and $\exp[-W_{\mu}(\mathbf{Q})]$ the Debye-Waller factor of atom μ. $\mathbf{v}_{\mu}(\mathbf{q}\lambda)$ denotes the eigenvector of the normal mode.

We now consider the situation where the unit-cell contains N_M C_{60} molecules whose centers are situated at $\mathbf{R}_m$, $m=1\cdots N_M$. If the orientation of each molecule is described by a rotation matrix D_m with respect to a reference orientation, the position vector of an atom is given by

$$\mathbf{R}_{\mu}=\mathbf{R}_m+D_m\mathbf{R}_{\kappa}^{(0)}, \tag{3}$$

where $\mathbf{R}_{\kappa}^{(0)}$, $\kappa=1\cdots 60$ are the corresponding position vectors of the carbon atoms of a single C_{60} molecule in the reference orientation.

When the interactions between molecular units are very weak, their influence on the internal vibrations may be neglected. Each normal mode ν of an isolated molecule with frequency ω_{ν} and eigenvector $\mathbf{v}_{\kappa}^{(0)}(\nu)$ in the reference orientation gives rise to N_M dispersionless phonon branches, $\lambda=\nu_m$, with eigenvectors $\mathbf{v}_{m'\kappa}(\nu_m)=\delta_{m,m'}D_m\mathbf{v}_{\kappa}^{(0)}$. Because frequencies and eigenvectors of internal vibrations are independent of $\mathbf{q}$, the momentum summation in Eq. (1) can be carried out easily. We further make the simplifying assumption that the Debye-Waller factor is isotropic and is the same for all atoms (we note that the Debye-Waller factor was close to unity in our case, as the experiments were carried out at very low temperatures, so that our simplifying assumptions for the Debye-Waller factor are of very little influence on the calculated results). The scattering cross section can then be written as a sum of contributions from different molecules:

$$\frac{d^2\sigma}{d\Omega dE}=\frac{k_f}{k_i}\frac{\pi^2\sigma_c}{v_0M}\frac{1+n(\omega)}{\omega}e^{-2W(Q)}Q^2 \times\sum_{\nu}\delta(\omega-\omega_{\nu})\sum_{m} S_{\nu}(D_m^{-1}\mathbf{Q}). \tag{4}$$

Coherence effects manifest themselves in

$$S_{\nu}(\mathbf{Q})=\left|\sum_{\kappa}\hat{\mathbf{Q}}\mathbf{v}_{\kappa}^{(0)}(\nu)e^{-i\mathbf{Q}\mathbf{R}_{\kappa}^{(0)}}\right|^2, \tag{5}$$

where $\hat{\mathbf{Q}}$ denotes the unit vector in the direction of $\mathbf{Q}$. Although coherence effects due to scattering off atoms belonging to different molecules are ignored in this approximation, Eq. (4) still contains information about the orientational order of the molecules, because the contribution from a molecule depends on its orientation with respect to the scattering momentum $\mathbf{Q}$.

For comparison with measurements on polycrystalline samples, Eq. (4) has to be averaged over all directions of $\mathbf{Q}$. One obtains for the powder-averaged partial differential cross section

$$\overline{\left(\frac{d^2\sigma}{d\Omega dE}\right)}=\frac{k_f}{k_i}\frac{\pi^2\sigma_c}{v_0M}\frac{1+n(\omega)}{\omega}e^{-2W(Q)}Q^2 \times\sum_{\nu}\delta(\omega-\omega_{\nu})N_M\overline{S_{\nu}(Q)} \tag{6}$$

with

$$\overline{S_{\nu}(Q)}=\int\frac{d\Omega_Q}{4\pi}S_{\nu}(\mathbf{Q})=\frac{1}{3}+\sum_{\kappa\neq\kappa'}\{\mathbf{v}_{\kappa}^{(0)}(\nu)\mathbf{v}_{\kappa'}^{(0)}(\nu)f_1(x_{\kappa\kappa'}) +(\mathbf{v}_{\kappa}^{(0)}(\nu)\hat{\mathbf{R}}_{\kappa\kappa'})(\mathbf{v}_{\kappa'}^{(0)}(\nu)\hat{\mathbf{R}}_{\kappa\kappa'})f_2(x_{\kappa\kappa'})\}. \tag{7}$$

Here, $\mathbf{R}_{\kappa\kappa'}=\mathbf{R}_{\kappa}-\mathbf{R}_{\kappa'}$, $\hat{\mathbf{R}}_{\kappa\kappa'}=\mathbf{R}_{\kappa\kappa'}/|\mathbf{R}_{\kappa\kappa'}|$, and $x_{\kappa\kappa'}=|\mathbf{Q}||\mathbf{R}_{\kappa\kappa'}|$. The Q dependence is contained in the structure functions f_1 and f_2, which can be expressed in terms of spherical Bessel functions as $f_1(x)=j_1(x)/x=(\sin x-x\cos x)/x^3$ and $f_2(x)=-j_2(x)=[(x^2-3)\sin x+3x\cos x]/x^3$. They still incorporate effects due to coherent scattering within a single molecule, but do not depend any more on the relative orientation of the C_{60} molecules.

C. Modeling of the $H_g(1)$ dispersion

For our investigation of the $H_g(1)$ dispersion, we require a reliable model of the intermolecular interaction. Until now, no *ab initio* calculation is available, but several phenomenological models have been proposed.[33,34] They are based on atom-atom potentials and usually consist of a van der Waals (vdW) interaction (mostly described by a Lennard-Jones potential) and secondary interactions, which are most often modeled by Coulomb interactions between point charges placed on the C-C bonds or on the atom sites. The secondary interactions are needed to accurately describe the orientation dependent part of the intermolecular interaction, and is known to strongly affect the librational spectrum. On the other hand, it has only a marginal influence on external modes with translational character, which are predominantly determined by the radial dependent part of the interaction.

As will be demonstrated in Sec. IV, the main experimental findings concerning the $H_g(1)$ dispersion can be already well accounted for by a less sophisticated model for the intermolecular interaction, which consists of a combination of the force-constant model of Jishi *et al.* and the Lennard-Jones potential proposed by Lu *et al.*[34] (with parameters $\epsilon=2.8486$ meV and $\sigma=3.407$ Å). Figure 2 shows the dispersion of the formerly fivefold degenerate $H_g(1)$ manifold as obtained for a fully ordered $Pa\bar{3}$ phase, where all the molecules sit in the ground-state (''pentagon'') orientation with rotation angle 100° away from the standard orientation. Structure factors discussed in Sec. IV have been calculated on the basis of Eq. (1).

There are two arguments which justify our simplified approach: (i) as will be shown below, the eigenvectors of the $H_g(1)$ mode as predicted by the phenomenological model are practically identical to those obtained in the *ab initio* calculation. (ii) apart from a scale factor, our calculated dispersion curves of the $H_g(1)$ manifold has a very similar shape as those obtained by Yu *et al.* and Pintschovius and Chaplot,[35,36] who used a combined vdW and Coulomb potential with charges sitting on the bonds. Within our model,

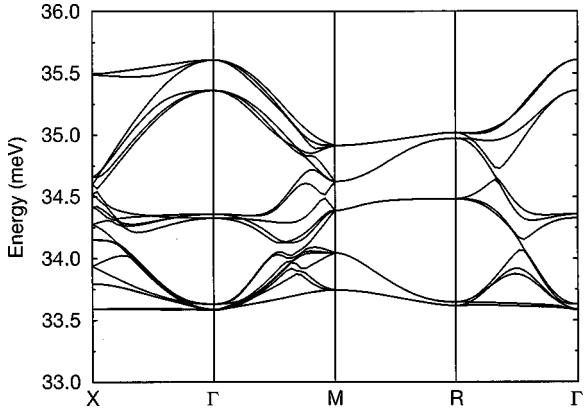

FIG. 2. Dispersion of $H_g(1)$-related modes as calculated from a model with the ansatz of Jishi *et al.* (Ref. 13) for the intramolecular interactions and the vdW potential taken from Ref. 34 for the intermolecular interactions. The structure was assumed to be fully ordered with all the molecules being in the pentagon orientation.

the same topology of the dispersion curves is also found for a fully ordered hexagon phase ($Pa\bar{3}$ rotation angle 40°). These similarities suggest that the main features of the $H_g(1)$ dispersion are determined by the vdW interaction alone, whereas details of the angle-dependent interaction as well as the orientation of the molecules have only a small influence.

III. EXPERIMENTAL METHODS

Experiments were performed both on a powder sample and on a single crystal. The powder sample consisted of three grams of fine grained C_{60} (purchased from the Hoechst Company, super gold grade), compacted to pellets of 5 mm height and 12 mm diameter which were encapsulated in an aluminum container. In order to reduce the amount of multiple scattering the pellets were separated from each other by Gd discs.

The single crystal was grown from the vapor phase and had a volume of 0.1 cm^3 ($m=0.227$ g). Details of the crystal growth procedure are described elsewhere.[37] The crystal was nearly single domain: additional domains were found to have a volume of not more than $\sim 0.1\%$. The sample was mounted with an 110-axis vertical.

The experiments were performed on the 2T-triple-axis spectrometer located at the ORPHEE reactor of the LLB of Saclay. Horizontally and vertically focusing crystals were used as monochromator and analyzer. For the measurements on the powder sample a Cu220 crystal was used as monochromator giving an energy resolution of $\Delta E/E=2.4$ to 3.5% in the energy range $E_0=48$–85 meV. For the sake of a higher intensity a Cu111 crystal was used as monochromator for the measurements on the single crystal giving an energy resolution $\Delta E/E=3.4$ to 4% in the energy range 48–66 meV. A PG002 crystal was used as analyzer in all cases. Most measurements were performed with a final energy $E_F=13.4$ meV and a PG filter placed in the scattered beam to suppress higher-order contaminations. In order to minimize contributions from multiphonon scattering and to minimize the effect of the Debye-Waller factor all experiments were carried out at the lowest temperature accessible with our closed-cycle refrigerator, i.e., $T=12$ K.

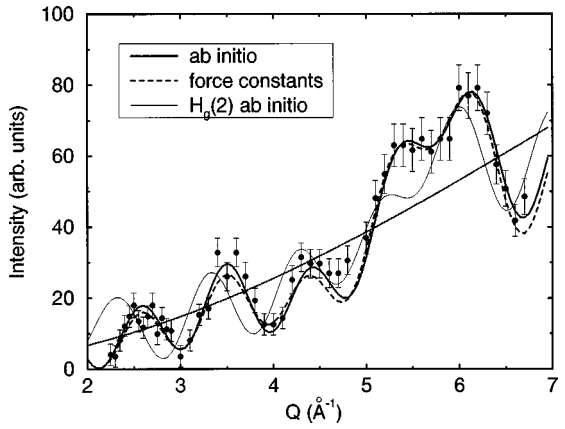

FIG. 3. Background and multiple-scattering-corrected scattering intensity at $E=33$ meV versus momentum transfer as observed on a powder sample at $T=12$ K. The heavy and light full lines correspond to the prediction of the *ab initio* theory (Ref. 10) for the $H_g(1)$ and the $H_g(2)$ mode, respectively, with the scaling as the only parameter. The dashed line shows the corresponding prediction of the force-constant model (Ref. 13) for $H_g(1)$ mode. The dotted line illustrates the simple Q^2 behavior. In the calculations allowance was made for the Debye-Waller factor deduced from the vibrational spectrum, i.e., $2W=Q^2 0.004$ Å^2.

IV. RESULTS AND ANALYSIS

A. $H_g(1)$ mode

1. Powder sample

The momentum dependence of the intensity of the 33 meV peak observed on the powder sample is plotted in Fig. 3. The data were corrected for background scattering as interpolated from the scattering at $E=30$ meV and $E=36$ meV, respectively. In addition, a constant amount of 10 in units of Fig. 3 was subtracted from all observed values to account for multiple-scattering events. As was mentioned in Sec. III, the sample had been sectioned to reduce multiple-scattering contributions. However, estimates showed that this precaution was not sufficient to reduce multiple-scattering contributions to negligible levels, and that further attempts to substantially reduce multiple-scattering contributions would lead to very low counting rates. As a consequence, we had to resort to a correction procedure. In principle, multiple-scattering contributions can be computed by a Monte Carlo technique but it would have required a large computational effort to model the multiple-scattering events for the actual sample geometry with sufficient accuracy. Therefore, we adopted the simplified procedure mentioned above guided by the idea that multiple scattering will certainly not show much, if any Q dependence. The extent of the correction was chosen so as to make the data shown in Fig. 3 and with a corresponding correction the data shown in Fig. 11 follow the general Q^2 behavior. The multiple-scattering contributions determined by this manner are fully in line with what was expected from calculations using a simplified geometry. The scaling factor was determined by a fit to the data, whereby we aimed at simultaneously describing the data for the $H_g(1)$ mode and those for other modes depicted in Fig. 11.

Figure 3 demonstrates that the scattering intensity does not follow a simple Q^2 behavior which can be exploited to obtain information on the mode eigenvector. There is a general consensus that this mode, which is Raman active, is the lowest of the H_g modes. Therefore, it was obvious to compare the observed Q dependence with that calculated for the $H_g(1)$ mode on the basis of the *ab initio* theory (Ref. 10) and the force-constant model (Ref. 13) introduced in Sec. II. There is obviously very good agreement between theory and experiment whereby it is difficult to discriminate between the two theories although a slight preference may be seen in favor of the *ab initio* results. Of course, the confirmation of the generally accepted assignment of the 33 meV peak does not come as a surprise. In order to assess the importance of the agreement between theory and experiment we made a further check: we compared the experimentally observed Q dependence with that expected for the $H_g(2)$ mode (light full line in Fig. 3). Although there is no reason to doubt that the 33 meV peak is associated with a H_g mode it is not so obvious that it is just the calculated pattern of the $H_g(1)$ mode which fits to the experiment, and not that of the next highest H_g mode or a mixture of them. Clearly, the agreement between calculation and experiment is very much in favor of the $H_g(1)$ mode confirming all the more the common assignment of the 33 meV-peak.

As will be shown below neither the very good agreement between the predictions of the two theories under consideration nor between theory and experiment is a matter of course. Presumably, the eigenvector of the $H_g(1)$ mode is particularly easy to predict as there is a large energy difference between the $H_g(1)$ mode and the next highest one, so that any physically plausible ansatz for the interatomic force field in conjunction with the molecular geometry will lead to a satisfactory description of the $H_g(1)$ mode eigenvector.

Copley *et al.*[30] found that the intensity of the 33 meV peak in the energy distribution of neutrons scattered from solid C_{60} by the beryllium detector method was too low by a factor ~ 2 when compared to calculated spectra. On the basis of a comparison with results of Coulombeau *et al.*[28] obtained by a time-of-flight method, Copley *et al.* concluded that coherency effects rather than possible errors in the calculated eigenvectors are the source of this discrepancy. This view is fully confirmed by our own results: in the beryllium detector experiment the 33 meV peak was sampled at $Q=4.05$ Å^{-1} (in such an experiment there is a very close relationship between the energy and the momentum transfer), which corresponds to a local minimum in the scattering cross section (see Fig. 3).

2. Single-crystal sample

Measurements on a single-crystal sample allow one to study the direction dependence of the scattering cross section. For $Q \leqslant 3$ Å^{-1} the direction dependence is rather small: for very small Q the C_{60} molecules behave as hollow spheres. For large Q, however, the atomic arrangement on the molecular surface does lead to a marked direction dependence of the scattering cross section. Unfortunately, this direction dependence is somewhat damped due to the unavoidable orientational disorder in C_{60} samples even at the lowest temperatures.[38] In our simulations, this orientational disorder was taken into account by calculating the weighted average

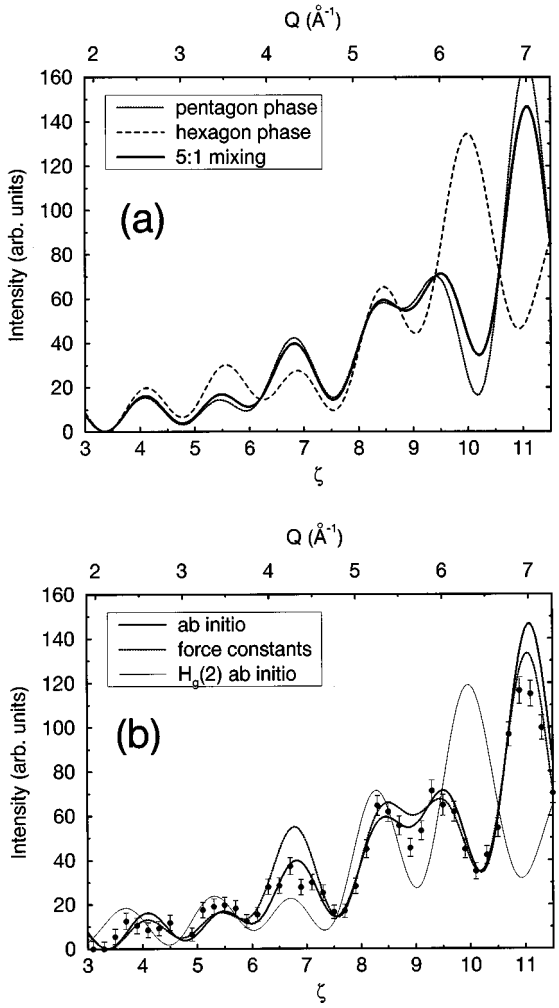

FIG. 4. (a) Intensity of the 33 meV peak versus momentum transfer $(\zeta,\zeta,0)$ observed on a single-crystal sample at $T=12$ K. The light full and dotted lines show the prediction of the *ab initio* theory (Ref. 10) for a pure pentagon or hexagon phase, respectively. The heavy line shows the result for a 5:1 mixing of the two phases. (b) The heavy full and dotted lines denote the predictions of the *ab initio* theory (Ref. 10) and the force-constant model (Ref. 13) for the $H_g(1)$ mode, respectively, and the light line shows the prediction of the *ab initio* theory for the $H_g(2)$ mode using the same scaling.

for a phase where all the intermolecular contacts are pentagon-double-bond (weight 5) or hexagon-double-bond (weight 1), respectively. The weights correspond to the results of David *et al.*[39] for temperatures below the glass transition. The large predominance of the pentagon fraction ensures that the direction dependence expected for a pure pentagon phase is not strongly washed out by the orientational disorder [see Fig. 4(a)].

Figure 4(b) shows the momentum dependence of the scattering cross section along a particular crystallographic direction, namely (110). A comparison with Fig. 3 reveals that local minima and local maxima occur in general at approximately the same positions, but with different relative heights. It is only at the upper end of the momentum range investigated that there is no longer a close correspondence between minima and maxima observed as a direction average or along (110) (at $Q \approx 6.8$ Å^{-1}, the single-crystal data show a large

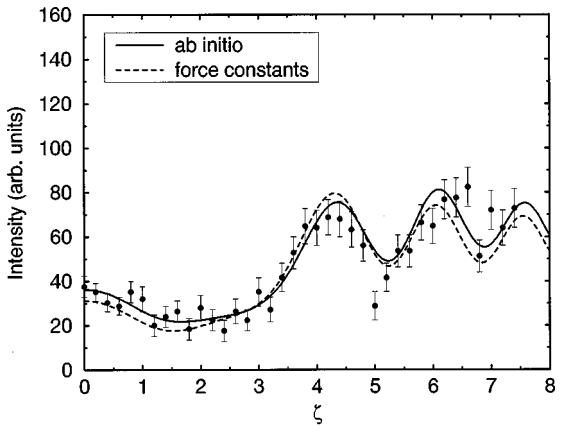

FIG. 5. The same as Fig. 4(b) but for the $(10,\zeta,\zeta)$ direction, using the same scaling.

peak, whereas the powder data show a local minimum).

When comparing the data to the theoretical results we find that (i) the predictions of the *ab initio* theory[10] and the force-constant model[13] differ more from each other than is the case for the direction averaged cross section, and (ii) that the agreement between theory and experiment, although still satisfactory, is not as good as was found for the powder data. We conclude that a comparison to single-crystal data constitutes a more stringent check of theoretical results than a comparison to powder data.

The question is, how serious are the discrepancies between theory and experiment apparent in Fig. 4(b)? We tried to find a better set of eigenvectors than those originally computed from the *ab initio* theory by admixing a certain amount of the eigenvectors of the $H_g(2)$ mode (assuming that admixtures of even higher H_g modes can be probably ignored). However, we soon realized that finding an appropriate linear combination of eigenvectors which fits to the crystal symmetry and improves the agreement between theory and experiment is very cumbersome. So, we arrived only at a qualitative conclusion, that the discrepancy seen in Fig. 4(b) can be explained by an admixture of about 10% of the calculated $H_g(2)$ eigenvectors to the calculated $H_g(1)$ eigenvectors, i.e., by a normalized eigenvector of the form $0.995\ H_g(1) + 0.1\ H_g(2)$. We note that the change in frequency associated with such an admixture is not very important: it is only (0.1^2) times the frequency difference between the $H_g(1)$ and the $H_g(2)$ modes, i.e., about 0.2 meV. In other words, the good agreement between calculated and experimental $H_g(1)$ energies is not put into question by our finding that the calculated $H_g(1)$ eigenvectors are not fully consistent with our experimental results.

The direction dependence of the scattering cross section is more directly probed by transverse scans. We made scans in the $(10,\zeta,\zeta)$ and the $(13,\zeta,\zeta)$ directions because we anticipated particularly pronounced structures in these directions on the basis of the theoretical predictions. Again, we found satisfactory, although not perfect, agreement between theory and experiment, as is illustrated for the $(10,\zeta,\zeta)$ direction in Fig. 5.

So far we ignored all the splittings and the dispersion induced by the intermolecular interactions and considered only the sum of the phonon branches depicted in Fig. 2. We tried to check the results of our simple ansatz to represent the intermolecular interactions by a vdW potential by making measurements at many different points in reciprocal space. Calculations of inelastic structure factors told us that it was practically impossible to follow the dispersion of individual branches because of unfavorable selection rules, and so we restricted our measurements to the high-symmetry points Γ, X, M, and R. The Q points were selected as to give reasonable counting rates (which meant $Q \geq 4$ Å^{-1} and medium to large structure factors), and further to sample predominantly high- or low-frequency modes or both at the same time. The results of this investigation are shown in Fig. 6. As theoretical peak positions we have taken the average of mode frequencies weighted by their structure factors. As can be seen from Fig. 6(a) the correlation between calculated and observed frequencies is not fully satisfactory (hereby we leave out of consideration the general offset between calculated and observed energies which is due to an imperfect modeling of the intramolecular forces by the ansatz of Jishi *et al.*[13]) We note that the finite momentum resolution was taken into account in calculating the energies, so resolution effects can be left out in the following discussion. The rather low slope of the straight line (0.59 ± 0.10) obtained by a linear regression analysis suggests that the calculation overestimates the total dispersion. However, Raman results reported by Horoyski *et al.*[19] and Hamanaka *et al.*[20] indicate that the splitting at Γ is not much smaller than calculated by our model, i.e., $\Delta E_{\max} = 1.75$ meV instead of 2.0 meV, so that a general down scaling of the calculated dispersion by a factor 0.88 would only partly remedy the discrepancy.

A loose correlation between calculated and observed energies may be due to incorrect predictions of frequencies or to incorrect predictions of structure factors. We found that the calculated total cross sections are in relatively good agreement with experiment [see Fig. 6(b)], although a linear regression analysis showed again some deviation from the expected behavior. Likewise, the observed peak widths were in approximate but not full agreement with the model calculations [Fig. 6(c)].

When searching for the reasons for the somewhat unsatisfactory agreement between model and experiment we came to consider the effects of the rotational disorder present in our sample but ignored in our calculation. This rotational disorder will affect both the energies and the intensities. Unfortunately, calculations using large supercells to realistically model the rotational disorder are far beyond the capabilities of present day computers. In order to assess the influence of the rotational disorder in a qualitative way we performed additional calculations for a pure hexagon phase. From these results we learned the following: the dispersion curves of the hexagon phase look rather similar to those of the pentagon phase but the overall dispersion calculated for the same lattice parameter is reduced by 20%. We presume that this is related to the well-known fact that hexagon-oriented C_{60} molecules need less space than pentagon-oriented molecules. The sizeable difference between the dispersion of the two phases implies that rotational disorder entails a significant force-constant disorder, so that it cannot be expected that the lattice vibrations are fully described in the picture of the virtual crystal approximation.

When the quantities displayed in Fig. 6 are recalculated for a 5:1 mixture of the pentagon and the hexagon phases in

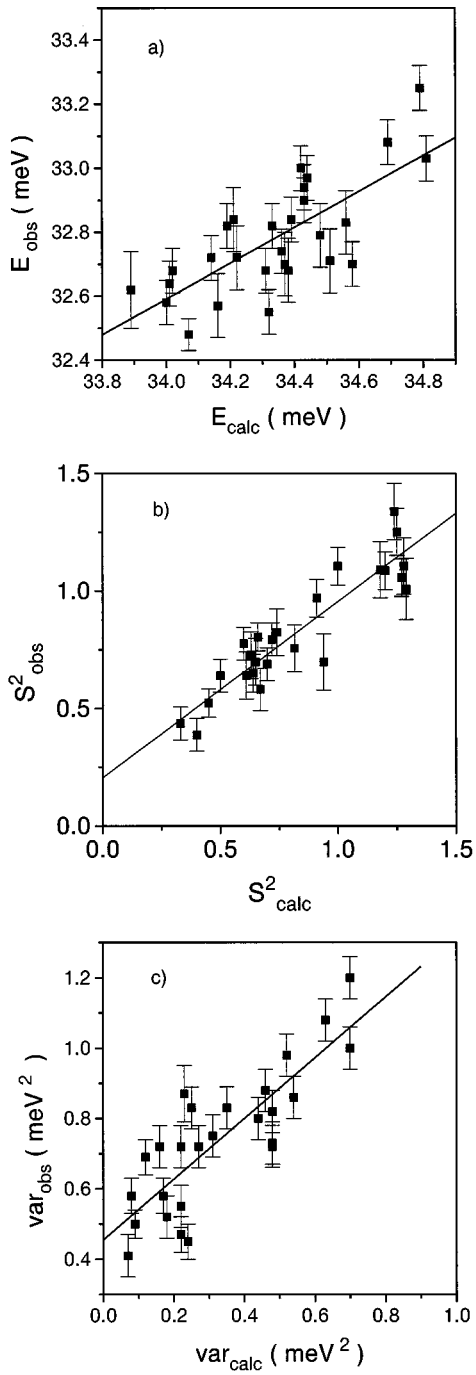

FIG. 6. (a) Observed versus calculated positions of peaks associated with $H_g(1)$-related modes for various high-symmetry points in reciprocal space. (b) Observed versus calculated total cross section of the same modes. (c) Observed versus calculated variance of the peaks of part (a). Calculations were performed for a fully ordered pentagon phase. Lines denote results of a linear regression analysis.

the incoherent approximation the agreement between experiment and theory is indeed improved. In particular, the observed cross section becomes nearly proportional to the calculated total cross section of all the modes, the remaining deviations being within experimental errors. However, it is not very surprising that the incoherent approximation works quite well for the total cross section of all $H_g(1)$-related modes. The incoherent approximation will certainly be less satisfactory for the scattering cross sections of individual modes which show very large differences between the two phases.

The correlation between calculated and observed frequencies remains somewhat unsatisfactory after allowance is made for the rotational disorder. Presumably, this indicates that the vdW potential is not fully appropriate for describing the dispersion of internal modes, although caution is advisable in view of the incoherent approximation used in our study. A certain inadequacy of the vdW potential for reproducing the dispersion of internal modes would not come as a surprise in view of the poor description of external modes with librational character by this potential (a factor 5 in terms of force constants[36]). Rather, one might be surprised that on the whole the vdW potential works fairly well for describing the dispersion of the internal modes. We think that this is related to the fact that the $H_g(1)$-related vibrations with predominant radial character demand not so much on the orientational part of the potential rather than on the radial one, which is relatively well described by the vdW ansatz.

In summary, we conclude that the dispersion of $H_g(1)$-related modes as obtained with the vdW potential provides a rather satisfactory description of our data when allowance is made for the unavoidable rotational disorder, but that the dispersion of internal modes is not a good testing ground for the intermolecular potential due to the smallness of the dispersion, to unfavorable selection rules, and last but not least to disorder effects.

B. Modes at $E \approx 43$ meV

In inelastic-scattering experiments on powders[28,30] a peak was observed at $E \approx 43$ meV which was somewhat broader than the experimental resolution. Therefore, the peak was attributed to two modes of slightly different energy, i.e., a G_u mode at $E = 42.6$ meV and a H_u mode at $E = 44.0$ meV by Coulombeau *et al.*[28] or a T_{2u} mode at $E = 42.6$ meV and a G_u mode at $E = 43.6$ meV by Copley *et al.*[30] We note that the results of Jishi *et al.*[13] suggest an assignment of this peak to a T_{2u} and a H_u mode, whereas the *ab initio* results strongly favor the assignment made by Copley *et al.*[30] (this seems to have been their basis of the assignment). As will be shown in the next paragraph we found compelling evidence that the lowest H_u mode is at $E = 49$ meV, so that the choice for the two modes in question was narrowed down to the $T_{2u}(1)$ and the $G_u(1)$ mode. A calculation of the direction-averaged cross section showed a very similar Q dependence for these two modes. Hence, powder measurements are inappropriate to decide which mode has the higher energy and by how much. On the other hand, single-crystal measurements do offer an opportunity to pin down the two modes separately due to favorable selection rules. Figure 7 shows the results of two measurements at different points in reciprocal space for which the *ab initio* theory[10] predicts that the cross section is dominated to more than 90% by either the $G_u(1)$ mode $[Q=(13,1,1)]$ or the $T_{2u}(1)$ mode $[Q=(0,9,9)]$, respectively.

From these measurements it follows that the $G_u(1)$ mode is higher in energy by nearly 1 meV, in very good agreement with *ab initio* results (see Table I). The average frequency of

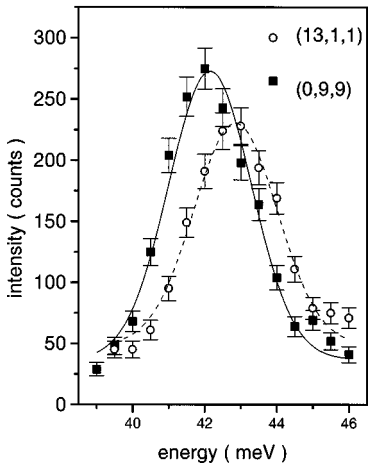

FIG. 7. Energy scans performed at Q points where theory predicts that the scattering cross section is dominated by the $G_u(1)$ mode $[Q=(13,1,1)]$ or the $T_{2u}(1)$ mode $[Q=(0,9,9)]$, respectively.

the two modes derived from our measurements is slightly lower than that obtained by Coulombeau *et al.*[28] and Copley *et al.*,[30] which very probably reflects a slightly different calibration. Results of second-order Raman scattering[40] favor the higher value, whereas photoluminescence results[41] favor the lower one.

The overlap of the $T_{2u}(1)$ and the $G_u(1)$ peaks hampers attempts to check the theoretically predicted eigenvectors. Still, some valuable checks can be made, and the result of such an investigation is shown in Fig. 8. Theory predicts that in the direction investigated the scattering cross section for the $T_{2u}(1)$ mode is much larger than that for the $G_u(1)$ mode. In addition, the $T_{2u}(1)$ contributions were favored over the $G_u(1)$ contributions by the choice of the energy in the const-

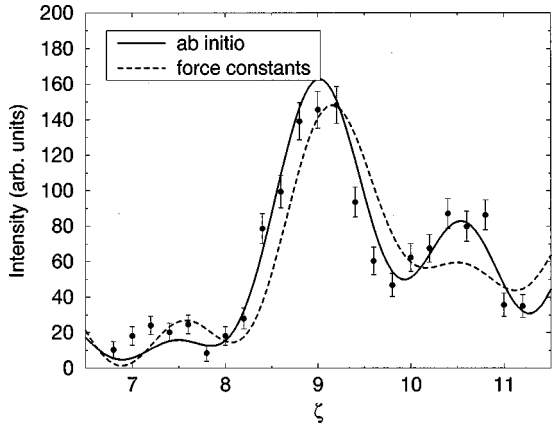

FIG. 8. Background-corrected intensity measured at $E=41.8$ meV versus momentum transfer $(\zeta,\zeta,0)$ observed at $T=12$ K. The dashed and broken lines correspond to the intensities calculated from the *ab initio* theory (Ref. 10) and the force-constant model (Ref. 13). The energy transfer chosen corresponds to the $T_{2u}(1)$ mode, but because of insufficient energy resolution contributions of the $G_u(1)$ mode are not fully suppressed. For this reason, the theoretical curves were calculated as the weighted sum $I(T_{2u})+0.5\,I(G_u)$ of the contributions of the two modes in question, whereby the contributions from the $G_u(1)$ mode do not exceed 5% of the peak intensity.

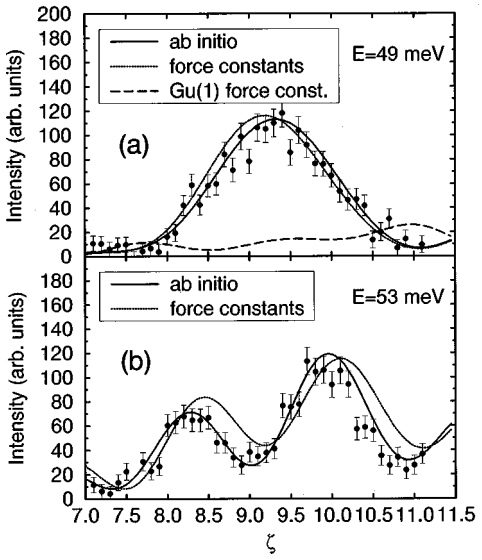

FIG. 9. Intensity of the 49 meV peak (a) and of the 53 meV peak (b) versus momentum-transfer $(\zeta,\zeta,0)$ observed on a single crystal at $T=12$ K. The full and dotted lines correspond to the prediction of the *ab initio* theory (Ref. 10) and of the force-constant model (Ref. 13), respectively, for the $H_u(1)$ mode (a) and the $H_g(2)$ mode (b). We note that the frequencies calculated from the force-constant model suggest to associate the 49 meV peak not with the $H_u(1)$ mode, but with the $G_u(1)$ mode. The corresponding intensities are shown by the dashed line. The scaling is the same for all curves and based on more data sets than shown in the figures.

E scan, so that the results shown in Fig. 8 can be largely considered as a check of the $T_{2u}(1)$-mode eigenvector. Clearly, the Q-dependence predicted by the *ab initio* theory[10] is in very good agreement with experiment thereby confirming our interpretation of the results shown in Fig. 7. Further inspection of Fig. 8 shows that in this case the agreement between theory and experiment is significantly worse for the force-constant model.

C. $H_u(1)$ and $H_g(2)$ modes

The assignment of the 49 meV peak has been of some debate in the literature. Whereas almost all *ab initio* theories propose an identification as $H_u(1)$, certain phenomenological models predict a different association (cf. Table I). For example, the model of Jishi *et al.* suggests to assign the $G_u(1)$ mode to this peak.

Our single-crystal measurements unambiguously confirm the *ab initio* assignment. Figure 9 shows the momentum dependence of the intensity along the (110) direction for the 49 (above) and 53 meV peak (below), respectively, with the same scale factor used for both data sets. Very similar results have been obtained for scans along the (111) direction. From Raman experiments, the latter peak is known to be $H_g(2)$. The momentum dependence of its intensity is well described by the *ab initio* theory. The characteristic maximum at $\zeta\approx 9$ of the 49 meV peak is properly reproduced by the $H_u(1)$ eigenvector of both theoretical models. On the other hand, the $G_u(1)$ mode shows a very low intensity with an essentially featureless momentum dependence [long dashed line in Fig. 9(a)], thus excluding $G_u(1)$ as a candidate for the 49 meV peak.

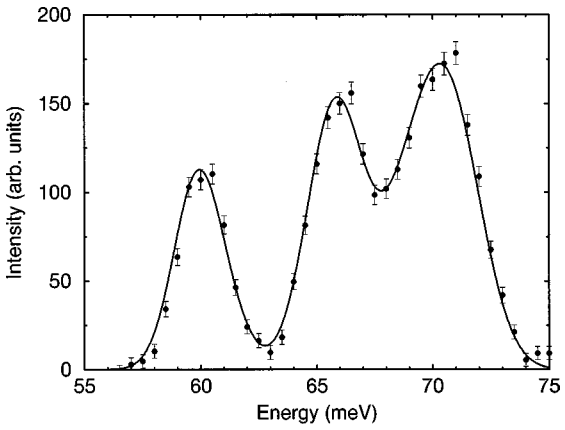

FIG. 10. Background-corrected intensity versus energy as observed on a powder sample at $T=12$ K. The data are the sum of several const-Q scans in the Q range 4–7.3 Å^{-1}. The line shows the result of a simulation of the experiment using the theoretically (Ref. 10) predicted mode energies and eigenvectors and the experimental resolution. Apart from the scale factor which was fitted to the data, small adjustments of the order of 1 meV (see text) had to be applied to the calculated mode energies to obtain the actual agreement between simulation and experiment.

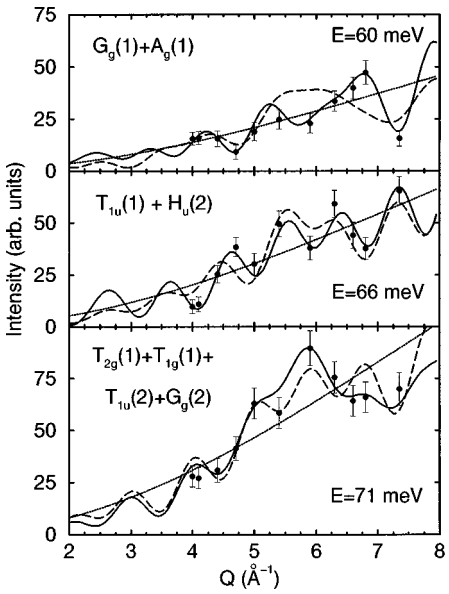

FIG. 11. Intensity versus momentum transfer of the 60 meV peak (above), the 66 meV peak (middle), and the 71 meV peak (below) as observed on a powder sample at $T=12$ K. The data were corrected for multiple-scattering effects. The full and dashed lines show the intensity variation predicted by the *ab initio* theory (Ref. 10) and the force-constant model (Ref. 13), whereas the dotted line shows the simple (Debye-Waller factor corrected) Q^2 behavior. The same scale factor was used for all the curves including those of Fig. 3.

As is seen from Fig. 9(b), the results of the phenomenological model for $H_g(2)$ describe the experimental data not as well as the *ab initio* theory, which indicates substantial differences in the corresponding eigenvectors. We found that the $H_g(2)$ eigenvectors predicted by the model of Jishi *et al.* incorporate about 30% of the eigenvectors of $H_g(3)$ predicted by the *ab initio* theory. This demonstrates that the phenomenological model is less reliable in predicting eigenvectors even for modes whose frequencies have been explicitly used to determine the parameters of the model.

D. Modes in the energy range 55–75 meV

As predicted by the *ab initio* theories, this frequency range should consist of eight modes which are separated energetically from the remaining spectrum by gaps of more than 7 meV. Due to our limited energy resolution, we could not resolve the individual modes but observe three groups of phonons. Figure 10 shows the measured intensity as a function of energy as obtained on a powder sample. The presented data are the sum of several constant-Q scans with Q ranging from 4 to 7.3 Å^{-1}.

According to the *ab initio* model,[10] the peak at 60 meV can be assigned to $A_g(1)$ and $G_g(1)$ and the second peak to $T_{1u}(1)$ and $H_u(2)$. The third peak should be attributed to four modes, $T_{2g}(1)$, $T_{1g}(1)$, $T_{1u}(2)$, and $G_g(2)$, respectively. A simulation of the experimental data using frequencies and eigenvectors predicted by this model reproduces correctly the total weights of the three phonon groups, but differs from the data in the detailed energy dependence. We tried to improve the model by slightly adjusting the mode frequencies. The best agreement with experiment has been obtained by (i) using frequencies from Raman and IR measurements for the optically active modes [$A_g(1)$, $T_{1u}(1)$, and $T_{1u}(2)$], and (ii) by applying additional frequency shifts of 1 to 2 meV to three other modes [$G_g(1)$, $H_u(2)$, and $T_{2g}(1)$]. The mode frequencies obtained by this procedure are listed in Table I, whereas the corresponding energy dependence of the intensity is given by the solid line in Fig. 10.

A more sensitive test of the proposed mode assignments is provided by the momentum dependence of the intensity of each individual phonon group. A comparison between experiment and theory is presented in Fig. 11. The very good agreement gives strong support for the proposed association, although we cannot exclude the possibility of an exchange of closely related modes within a group [e.g., $T_{1g}(1)$ and $T_{2g}(1)$]. For the phenomenological model (dashed lines in Fig. 11), however, obvious discrepancies for momenta close to $Q=6$ Å^{-1} exist. They are especially pronounced for the first phonon group (60 meV peak), where they can be attributed to the $G_g(1)$ mode, because the $A_g(1)$ mode gives only a small contribution to the total peak intensity ($<20\%$). When searching for the reason for this discrepancy we became aware that the $G_g(1)$ eigenvectors of the phenomenological model are an almost 1:1 mixture of the *ab initio* eigenvectors of $G_g(1)$ and $G_g(2)$. A similar hybridization is found for the phenomenological $G_g(2)$ mode which provides an explanation for the differences between the two theoretical models with regard to the third phonon group. Here, the deviations from experimental data are less pronounced because of substantial contributions to the total intensity coming from the three other modes of this group.

V. CONCLUSIONS

We have demonstrated that inelastic neutron scattering is a powerful technique to obtain detailed information on the eigenvectors of the intramolecular vibrations in solid C_{60}. The first important result of a study like ours is an unam-

biguous assignment of the silent modes. Our view that the assignment is far from being trivial is corroborated by our finding that in the tables published by Dong *et al.* (Ref. 40), Martin *et al.* (Ref. 42), and Wang *et al.* (Ref. 22) several experimental frequencies are assigned incorrectly. Being aware that the assignment is a nontrivial problem, groups like Jishi *et al.* refrained from using silent mode frequencies as input data — with the consequence that the silent modes are not as well reproduced by their model as the optically active modes. Very probably, better model parameters could have been found in case our results would have been available to Jishi *et al.*

The assignment is often seen as a clear-cut yes or no problem. However, this is not really true as, in general, eigenvectors are not determined by symmetry alone. We have demonstrated that eigenvectors derived from different theories may differ significantly, and that inelastic neutron scattering is able to tell which eigenvector is in satisfactory agreement with experiment and which is not.

We have found that a state-of-the-art *ab initio* study of the internal modes in C_{60} gives an extremely satisfactory description not only of the frequencies but also of the eigenvectors. It is true that the agreement between the predicted and the experimentally observed Q dependence of the intensities is not always perfect, but we consider the deviations as not very serious: estimates showed that the errors in the mode eigenvectors correspond to errors in the mode frequencies of the order of 1% only. As a consequence, claims made on the basis of a comparison of experimental and theoretical frequencies are not jeopardized. The *ab initio* theory[10] is clearly superior to the phenomenological theory of Jishi *et al.*[13] This does not mean that phenomenological models are generally unable to reproduce the C_{60} vibrations with sufficient accuracy. However, it does mean that it is very difficult if not impossible to construct such a model on the basis of a very limited data set. It is precisely one of the very advantages of an *ab initio* theory that it can be implemented at a time when little or no data are available.

At present, the very advanced state of our understanding of the intramolecular forces is in sharp contrast with our relatively poor understanding of the intermolecular forces. For the latter, only empirical potentials are available so far. We made an attempt to check the adequacy of a generally adopted simple ansatz, i.e., a vdW potential, and found fairly satisfactory agreement with experiment. The unavoidable rotational disorder in C_{60} samples is seen as a major obstacle for unraveling details of the phonon dispersion and thereby to check the adequacy of the vdW ansatz in a stringent way.

An experimental analysis of the eigenvectors of low-frequency internal phonons in a molecular solid was reported by Chaplot *et al.*[43] for crystalline anthracene. For this study, a fairly large single crystal was available, which is not very often the case for molecular solids, in particular not for other members of the fullerene family than just C_{60}. We emphasize that ''fairly large'' has to be seen in relation to the frequencies involved: the higher the frequencies the larger the required size of the crystals. Our C_{60} crystal was large enough only for the five lowest of the internal modes, and even for this frequency range it was large enough only because of the high luminosity of our spectrometer. However, we have shown that powder samples are sufficient to obtain a great deal of information on eigenvectors provided the data allow one to extract the Q dependence of the peak intensities with good accuracy. This has two important consequences for the planning of similar experiments on other molecular solids:

(i) instruments and instrumental parameters should be chosen not only in regard to high-energy resolution and high counting rates, but also in regard to the possibility to cover a large range in Q. From this viewpoint it follows that instrumental techniques using very low incident or final energies are not appropriate for the determination of mode eigenvectors.

(ii) Enough time should be allotted to the experiment to achieve good statistics not only for the Q-integrated spectrum but also for Q-decomposed spectra.

As a prerequisite, the molecular solid under investigation should possess two properties: (i) the characteristic energies for the internal and external modes are well separated, and (ii) the intermolecular interaction is weak enough to lead to only weak dispersion of the internal modes, so that single modes or groups of a small number of modes can still be resolved in frequency. These conditions might be fulfilled for other members of the fullerene family, which due to their lower molecular symmetry provide an even richer testing ground than C_{60} for the various theoretical approaches to phonon dynamics.

*Present address: Max-Planck-Institut für Physik komplexer Systeme, Bayreuther Straße 40, Haus 16, D-01187 Dresden, Germany.

[1] H. W. Kroto, J. R. Heath, S. C. O'Brien, R. F. Curl, and R. E. Smalley, Nature (London) **318**, 162 (1985).

[2] W. Krätschmer, L. D. Lamb, K. Fostiropoulos, and D. R. Huffman, Nature (London) **347**, 354 (1990).

[3] G. B. Adams, J. B. Page, O. F. Sankey, K. Sinha, J. Menendez, and D. R. Huffman, Phys. Rev. B **44**, 4052 (1991).

[4] J. Kohanoff, W. Andreoni, and M. Parrinello, Phys. Rev. B **46**, 3671 (1992).

[5] X. Q. Wang, C. Z. Wang, and K. M. Ho, Phys. Rev. B **48**, 1884 (1993).

[6] A. A. Quong, M. R. Pederson, and J. L. Feldman, Solid State Commun. **87**, 535 (1993).

[7] J. C. R. Faulhaber, D. Y. K. Ko, and P. R. Briddon, Phys. Rev. B **48**, 661 (1993).

[8] R. Jones, C. D. Latham, M. I. Heggie, V. J. B. Torres, S. Öberg, and S. K. Estreicher, Philos. Mag. Lett. **65**, 291 (1992).

[9] P. Giannozzi and S. Baroni, J. Chem. Phys. **100**, 8537 (1994).

[10] K.-P. Bohnen, R. Heid, K.-M. Ho, and C. T. Chan, Phys. Rev. B **51**, 5805 (1995).

[11] D. E. Weeks and W. G. Harter, J. Chem. Phys. **90**, 4744 (1989).

[12] Z. C. Wu, D. A. Jelski, and T. F. George, Chem. Phys. Lett. **137**, 291 (1987); R. E. Stanton and M. D. Newton, J. Phys. Chem. **92**, 2141 (1988).

[13] R. A. Jishi, R. M. Mirie, and M. S. Dresselhaus, Phys. Rev. B **45**, 13 685 (1992); R. A. Jishi, R. M. Mirie, M. S. Dresselhaus, G. Dresselhaus, and P. C. Eklund, *ibid.* **48**, 5634 (1993).

[14] J. L. Feldman, J. Q. Broughton, L. L. Boyer, D. E. Reich, and M.

D. Kluge, Phys. Rev. B **46**, 12 731 (1992).
[15] G. Onida and G. Benedek, Europhys. Lett. **18**, 403 (1992).
[16] D. S. Bethume, G. Meijer, W. C. Tang, H. J. Rosen, W. G. Golden, H. Seki, C. A. Brown, and M. S. Derries, Chem. Phys. Lett. **179**, 181 (1991).
[17] M. G. Mitch, S. J. Chase, and J. S. Lannin, Phys. Rev. Lett. **68**, 883 (1992).
[18] P. Zhou, K. Wang, Y. Wang, P. C. Eklund, M. S. Dresselhaus, G. Dresselhaus, and R. A. Jishi, Phys. Rev. B **46**, 2595 (1992).
[19] P. J. Horoyski, M. L. W. Thewalt, and T. R. Anthony, Phys. Rev. Lett. **74**, 194 (1995); Phys. Rev. B **54**, 920 (1996).
[20] Y. Hamanaka, M. Norimoto, S. Nakashima, and M. Hangyo, J. Phys.: Condens. Matter **7**, 9913 (1995).
[21] H. Kuzmany, M. Matus, B. Burger, and J. Winter, Adv. Mater. **6**, 731 (1994).
[22] K.-A. Wang, A. M. Rao, P. C. Eklund, M. S. Dresselhaus, and G. Dresselhaus, Phys. Rev. B **48**, 11 375 (1993).
[23] C. C. Homes, P. J. Moroyski, M. L. W. Thewalt, and B. P. Clayman, Phys. Rev. B **49**, 7052 (1994).
[24] H. Kuzmany, R. Winkler, and T. Piechler, J. Phys.: Condens. Matter **7**, 6601 (1995).
[25] G. Gensterblum, J. J. Pireaux, P. A. Thiry, R. Candane, J. P. Vigneron, Ph. Lambin, A. A. Lucas, and W. Krätschmer, Phys. Rev. Lett. **67**, 2171 (1991).
[26] R. L. Cappeletti, J. R. D. Copley, W. A. Kamitakahara, F. Li, J. S. Lannin, and D. Ramage, Phys. Rev. Lett. **66**, 3261 (1991).
[27] K. Prassides, T. J. S. Dennis, J. P. Hare, J. Tomkinson, H. W. Kroto, R. Taylor, and D. R. M. Walton, Chem. Phys. Lett. **187**, 455 (1991).
[28] C. Coulombeau, H. Jobic, P. Bernier, C. Fabre, D. Schütz, and A. Rassat, J. Phys. Chem. **96**, 22 (1992); C. Coulombeau, H. Jobic, C. J. Carlile, S. M. Bennington, C. Fabre, and A. Rassat, Fullerene Sci. Technol. **2**, 247 (1994).
[29] F. Gompf, B. Renker, W. Schober, P. Adelmann, and R. Heid, J. Supercond. **7**, 643 (1994).
[30] J. R. D. Copley, D. A. Neumann, and W. A. Kamitakahara, Can. J. Phys. **73**, 763 (1995).
[31] M. Schlüter, M. Lannoo, M. Needels, G. A. Baraff, and D. Tomanek, J. Phys. Chem. Solids **53**, 1473 (1992).
[32] S. W. Lovesey, *Theory of Neutron Scattering from Condensed Matter* (Clarendon, Oxford, 1984), Vol. 1.
[33] M. Sprik, A. Cheng, and N. Klein, J. Chem. Phys. **96**, 2027 (1992).
[34] J. P. Lu, X. P. Li, and R. M. Martin, Phys. Rev. Lett. **68**, 1551 (1992).
[35] J. Yu, R. K. Kalia, and P. Vashista, Phys. Rev. B **49**, 5008 (1994).
[36] L. Pintschovius and S. L. Chaplot, Z. Phys. B **98**, 527 (1995).
[37] J. de Bruijn, A. Dworkin, H. Szwarc, J. Godard, R. Ceolin, C. Fabre, and A. Rassat, Europhys. Lett. **24**, 551 (1993).
[38] W. I. F. David, R. M. Ibberson, J. P. Hare, and K. Prassides, Europhys. Lett. **18**, 219 (1992).
[39] W. I. F. David, R. M. Ibberson, and T. Matsuo, Proc. R. Soc. London, Ser. A **442**, 129 (1993).
[40] Z.-H. Dong, P. Zhou, J. M. Holden, P. C. Eklund, M. S. Dresselhaus, and G. Dresselhaus, Phys. Rev. B **48**, 2862 (1993).
[41] M. K. Nissen, S. M. Wilson, and M. L. W. Thewalt, Phys. Rev. Lett. **69**, 2423 (1992).
[42] M. C. Martin, X. Du, J. Kwon, and L. Mihaly, Phys. Rev. B **50**, 173 (1994).
[43] S. L. Chaplot, G. S. Pawley, E. L. Bokhenkov, E. F. Sheka, B. Dorner, J. Kalus, V. K. Jindal, and I. Natkaniec, Chem. Phys. **57**, 407 (1981).